Clinical Description and Genetic Analysis of a Novel Familial Skeletal Dysplasia Characterized by High Bone Mass and Lucent Bone Lesions

Diana Ovejero[1], Natalia Garcia-Giralt[1], Núria Martínez-Gil[2], Raquel Rabionet[2], Susanna Balcells[2], Daniel Grinberg[2], Luis Pérez-Jurado[3], Xavier Nogués[1], Iñigo Etxebarria Foronda[4].

1 Musculoskeletal Research Group, IMIM (Hospital del Mar Medical Research Institute), Centro de Investigación Biomédica en Red en Fragilidad y Envejecimiento Saludable (CIBERFES), ISCIII, Barcelona, Spain.

2 Department of Genetics, Microbiology and Statistics, Faculty of Biology, Universitat de Barcelona, CIBERER, IBUB, IRSJD, Barcelona, Spain.

3. Universitat Pompeu Fabra, IMIM-Hospital del Mar and CIBERER-ISCIII, Barcelona, Spain

4. Traumatology and Orthopedic Surgery Department, Hospital Alto Deba, Gipuzkoa, Spain

Corresponding author: Diana Ovejero, Musculoskeletal Research Group, Hospital del Mar Medical Research Institute, 88 Aiguader street, Room 200.10, Barcelona, 08003, Spain;. Email: dovejero@imim.es; ORCID ID: https://orcid.org/0000-0003-1312-4750

HIGHLIGHTS

- A previously unreported familial skeletal dysplasia with a probable autosomal dominant inheritance pattern is described.
- This extremely unusual phenotype is mainly characterized by high bone mass and bone lucent lesions.
- Patients are paucisymptomatic
- Whole-exome sequencing of affected family members revealed rare variants in genes associated with bone biology including *SEMA4D, TBX18, PTCH1, PTK7,* and *ADGRE5.*

Declaration of interests: "None"

Abstract

High bone mass (HBM) disorders are a clinically and genetically heterogeneous subgroup of rare skeletal dysplasias. Here we present a case of a previously unreported familial skeletal dysplasia characterized by HBM and lucent bone lesions that we aimed to clinically characterize and genetically investigate. For phenotyping, we reviewed past clinical records and imaging tests, and performed physical examination (PE), bone densitometry, and mineral panels in affected individuals, including a male proband, his son and daughter, in addition to unaffected controls, including the proband's wife and brother. Affected individuals also underwent impact microindentation (IMI). In an effort to elucidate the disorder's molecular etiology, whole exome sequencing (WES) was performed in all individuals to filter for rare variants present only in affected ones. The cases displayed a unique skeletal phenotype with a mix of sclerotic features and lucent bone lesions, and high IMI values. Bone mineral density was very elevated in the proband and his daughter. The proband's daughter also exhibited idiopathic scoliosis (IS), in addition to mild thrombocytopenia and mild structural thyroid abnormalities, which were the only extra-skeletal abnormalities identified. WES analysis yielded 5 rare putative pathogenic variants in affected members in genes that are associated with bone metabolism including: *SEM4AD, TBX18, PTCH1, PTK7,* and *ADGRE5.* The *PTK7* variant appeared as possibly implicated in the development of IS while the *TBX18* and *SEMA4D* variants stood out as the strongest candidates for the lucent bone lesions and HBM, respectively, given their high predicted pathogenicity and putative role in bone biology. Variant functionality should be addressed in the future to assess their implication in skeletal metabolism as it is the first time that mutations in *TBX18* and *SEMA4D* have been associated to bone developmental lesions and mineral metabolism in a clinical setting.

Key words: genetic research, diseases/disorders related to bone, impact microindentation, cell tissue signaling-paracrine pathways

Abbreviations

BAP: bone-specific alkaline phosphatase

CTX: C-terminal telopeptide of type 1 collagen

ECLIA: electrochemiluminescence immunoassay

FN: femoral neck

HBM: high bone mass

Hh: hedgehog

IMI: impact microindentation

IS: idiopathic scoliosis

ITP: idiopathic thrombocytopenic purpura

JDP: Juvenile Paget Disease

LS: lumbar spine

MAS: McCune-Albright Syndrome

OC: osteocalcin

P1NP: procollagen 1 N-terminal peptide

PCP: planar cell polarity

PE: physical exam

PFD: polyostotic fibrous dysplasia

PTH: parathormone

TH: total hip

TSH: thyrotropin

WES: whole-exome sequencing

1. Introduction

High bone mass (HBM) disorders comprise a rare, clinically and genetically diverse group of skeletal dysplasias characterized by supraphysiological bone mass [1]. They typically result from mutations that lead to impaired bone resorption by diminishing the number or function of osteoclasts (osteopetroses), or by targeting and stimulating bone formation pathways, although other physiopathologic mechanisms have also been described [1]. In their latest report, the "Working Group on the Classification and Nomenclature of Skeletal Dysplasias" has classified these disorders into three categories including neonatal osteosclerotic dysplasias, osteopetroses, and other high bone mass disorders [2].

Although these disorders resemble each other in that they all feature increased bone mass, the clinical implications of each particular disease are considerably different. For instance, severity may range from neonatal lethality, as in most neonatal osteosclerotic dysplasias, to lack of associated symptoms as in osteopoikilosis. Distinctive clinical manifestations are also very varied and, in some cases, radically different, e.g., altered osteoclastic function in the osteopetroses leads to bone brittleness and increased fracture rate, while bone overgrowth in sclereostosis and van Buchem disease, is associated with important reductions in fracture risk, albeit often displaying severe complications such as nerve compressions [1].

Advances in sequencing technologies have aided tremendously in the elucidation of the underlying mutations responsible of these disorders, and consequently, provide insights into their physiopathology. However, the molecular etiology of many sporadic and ultrarare cases remain frequently pending. This not only affects the patient, as an appropriate classification of the disease may have an important impact on its clinical management, but also limits our understanding of skeletal physiology in general.

Here we present a familial case of a sclerosing bone dysplasia that also featured lucent bone lesions, representing a unique and, to our knowledge, previously unreported phenotype. Whole exome sequencing (WES) of the cases revealed mutations in interesting candidates including genes involved in homeobox transcription regulation, osteoblastic and osteoclastic functions, and in the bone-forming Wnt signaling pathway.

2. Subjects and Methods

2.1 Subjects

Three subjects within the same family including the proband, his son, and his daughter, who exhibited rare skeletal manifestations, underwent physical examination (PE), clinical history, revision of previous medical records (including imaging studies and laboratory tests), impact microindentation (IMI) , bone densitometry by dual-energy x-ray absorptiometry (DXA), a blood mineral panel, and whole exome sequencing (WES). Clinical history, revision of radiologic imaging, DXA, a mineral panel, and WES were also performed in the proband's wife (i.e., mother of the affected children), and the proband's brother, both of whom were unaffected (controls). Of note: the images and clinical history depicting the case were recently sent to several international experts on rare bone diseases, including experts from Skeletal Dysplasia Information and Diagnosis in Lausanne. A couple of experts found radiological similarities with Juvenile Paget Disease (JPD) [3], but this diagnosis was excluded given that the individuals we studied were paucisymptomatic (in contrast to the severe manifestations and early-onset clinical presentation seen in patients with JPD), had normal or close-to-normal levels of alkaline phosphatase, and lacked mutations in *TNFRSF11B*. Besides this potential differential diagnosis, no alternative diagnosis was contemplated. Thus, to our knowledge, this represents a novel skeletal phenotype.

Informed consent was obtained from all individuals who participated in the study. The study was approved by the Clinical Research Ethics Committee of Parc de Salut MAR according to the ethical code of the World Medical Association declaration of Helsinki.

2.2 Dual-energy x-ray absorptiometry (DXA)

Bone mineral density (BMD) was measured by DXA at the lumbar spine (L1-L4) (LS), femoral neck (FN), and total hip (TH). BMD was measured with a DXA densitometer QDR 4500 SL® (Hologic, Waltham, MA, USA), according to the manufacturer's recommendations. In our department, the *in vivo* coefficient of variation of this technique is 1.0% at LS, 1.60% at TH, and 1.65% at FN.

2.3 Mineral Panel

All individuals underwent a blood mineral panel that included calcium, phosphate, kidney function, tissue non-specific alkaline phosphatase, bone-specific alkaline phosphatase (BAP) (electrochemiluminescence immunoassay (ECLIA), Liaison BAP Ostase, DiaSorin, Stillwater, MN) , osteocalcin (OC) (ECLIA, Roche Elecsys, Roche Diagnostics, Mannheim, Germany), C-terminal telopeptide of type 1 collagen (CTX) (ECLIA, Elecsys Beta Crosslaps, Roche Diagnostics), procollagen 1 N-terminal peptide (P1NP) (ECLIA, Roche Elecsys, Roche Diagnostics), and vitamin D (competitive immunoluminometric direct assay with direct-coated magnetic microparticles, Elecsys 25(OH)D total II, Roche Diagnostics).

2.4 Impact Microindentation

IMI was performed on the affected individuals. This technique allows for the *in vivo* assessment of bone tissue mechanical characteristics [4]. It is based on the principle that the deeper a test probe penetrates into a cortical bone's outer surface, the less resistant is the bone tissue to a mechanical challenge. The procedure was performed with the OsteoProbe handheld device (Active Life Scientific; California, USA) by an expert operator. Details on the technique have been previously published [5]. Briefly, the skin is first disinfected, and local anesthesia is applied through the injection of lidocaine 1% at the periosteum. The test probe is then inserted perpendicularly to the bone. After at least 8 adequate measurements, the probe is applied on a polymethylmethacrylate calibration phantom for at least five additional measurements. Bone mineral strength index (BMSi), IMI's unitless output variable, is then calculated by measuring the ratio between the penetration of the probe into the bone and its penetration into the reference phantom. BMSi normality ranges from 70-80.

2.5 Whole exome sequencing (WES)

DNA from the family members was extracted from peripheral blood with the Wizard Genomic DNA Purification Kit (Promega, Madrid, Spain) and was used for WES in the Center for Genomic Regulation platform (CRG, Barcelona, Spain). Libraries were prepared using the NEBNext® DNA Library Prep Reagent Set for Illumina® kit (ref. E7370L) according to the manufacturer's protocol. Briefly, 1 ug of DNA was fragmented

to approximately 250-300 bp and subjected to end repair, addition of "A" bases to 3′ ends, ligation of NEB Next hairpin adapter and USER excision. Then libraries were amplified using partial Illumina adapter primers. All purification steps were performed using AgenCourt AMPure XP beads (Beckman Coulter).

For exome selection, the SureSelect XT workflow was followed. Briefly, 750 ng from each library with partial adapters were used for hybridization with the Human All Exon V6 capture library. After 18 hours of incubation at 65ºC, probe-bound DNA was pulled down using streptavidin beads (Dynabeads MyOne Streptavidin C1, Invitrogen) and was further amplified using indexed primers to allow for multiplexing and to get full-length adapters.

Final libraries were analyzed using Agilent DNA 1000 chip to estimate the quantity and check size distribution and were then quantified by qPCR using the KAPA Library Quantification Kit (ref. KK4835, KapaBiosystems). Libraries were loaded at 20 pM into one lane and were sequenced 2 x 125 on Illumina's Hiseq2500 at coverage of 75-100x with paired-end runs of 2x76 bp following the manufacturer's protocol. Images from the instrument were processed using the manufacturer's software to generate FASTQ sequence files.

2.6 Bioinformatics analysis

Raw sequencing reads in the FASTQ files were mapped with BWA-MEM version 0.7.17 to the GRCh38 reference genome (GATK bundle). Samples were processed using GATK version 4.1.4.0 following GATK best practices, which includes removal of duplicates, recalibration, variant calling and filtering with VQSR (variant quality score recalibration). Haplotype Caller in GVCF mode followed by joint calling with GenotypeGVCFs was used to perform the germline variant calling. The resulting VCF files were annotated with Variant Effect Predictor version 98.3 [6]. The database versions used were Ensembl DB version: 98, Genome assembly GRCh38.p12, GENCODE 31, RefSeq "2019-06-28(GCF_000001405.39_GRCh38.p13_genomic.gff)", Regulatory build 1, PolyPhen 2.2.2, SIFT 5.2.2, dbSNP 152, CADD GRCh38-v1.6, COSMIC 89, HGMD-PUBLIC 2018.4, ClinVar 2019-04, 1000 Genomes Phase 3 (remapped), NHLBI-ESP V2-SSA137 (remapped), gnomAD r2.1, exomes only (remapped).

2.7 Variant filtering and prioritization

Genetic variants were filtered according to the following premises: a) nonsynonymous change; b) shared variants among affected individuals under an autosomal dominant inheritance pattern; c) absent in unaffected individuals; c) Minor Allele Frequency < 0.001 in gnomAD 's non-Finnish European population; and d) not present in highly variable genes. Resulting variants were then submitted to Matchmaker Exchange, an online platform that integrates data from several genomic and phenotypic databases in an effort to help researchers and physicians identify other patients with variants in the same genes that are phenotypically alike [7].

2.8 *In silico* study of genetic variants

SIFT [8], PolyPheN [9], and Combined Annotation Dependent Depletion (CADD) [10] scores were used for prediction of variant pathogenicity, and PhastCons in vertebrates [11] to analyze for variant evolutionary conservation.

3. RESULTS

3.1 Clinical history and review of past medical record/imaging and new radiographic imaging

The proband and his children were all born at term from unrelated Caucasian parents. They did not report suffering any developmental abnormalities or exhibiting evident problems during growth. Intelligence was normal in all. A pedigree chart is displayed in Figure 1.

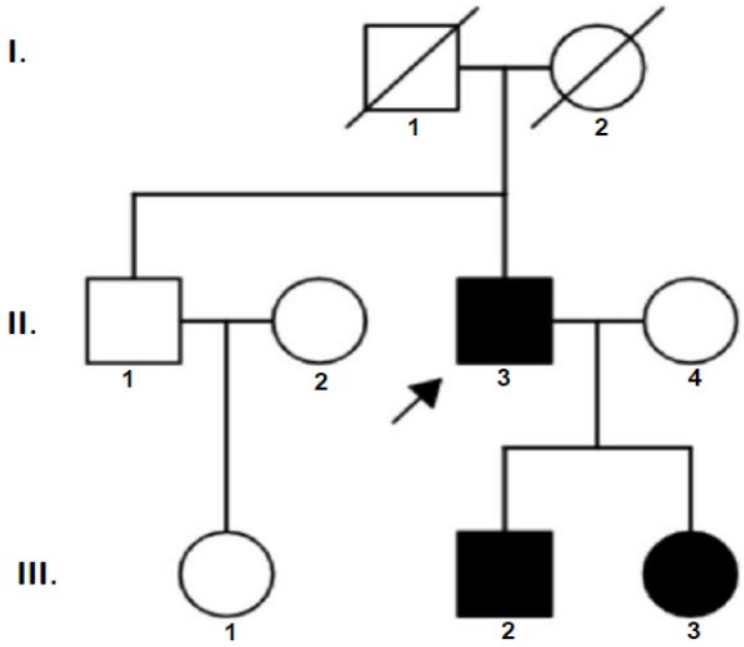

Figure 1. Pedigree of the family segregating a sclerosing skeletal dysplasia and lucent bone lesions. Black filled symbols indicate affected individuals. Whole exome sequencing was performed in individuals: II.1, II.3, II.4, III.2, and III.3

3.2 Proband

The proband was a 56-year-old man at the time of the study. He had not sustained any fractures during growth and young adulthood nor explained bone pain. At age 36, he fractured his proximal left humerus and femoral shaft in a car accident. Femoral and pelvic x-rays evidenced an abnormal periosteal reaction to the fracture, thickened femoral cortices in addition to rarefaction of the skeleton (Figure 2A), which led to subsequent imaging and laboratory studies. MRI of the pelvis and femurs also revealed diffuse rarefaction of the bone marrow signal which was also present in the left humerus (Figure 2B) and acromial base. In addition, MRI showed metaphyseal lucent lesions in the long bones that had been imaged i.e., proximal left humerus, proximal femurs, and distal right femur (knee MRI was requested for mechanical knee pain) (Figure 2C). A bone scan only revealed increased uptake around fractured areas. Blood tests showed

alkaline phosphatase, CRP, erythrocyte sedimentation rate, parathormone (PTH), thyrotropin (TSH), calcium, phosphorus, and complete blood count within the normal range. Serum protein electrophoresis, kidney and liver functions were also normal. Head CT performed at that time showed normal brain morphology without calcifications. At the time of the current study, the patient had developed mild type 2 diabetes mellitus (controlled through diet) and high blood pressure. The proband's parents were deceased at the time of the study: the father died of a stroke at age 74, and the mother died of ischemic heart disease at age 54. There was no known family history of fractures, or skeletal and mineral abnormalities. His brother, who did not explain any relevant medical history, underwent a radiographic skeletal survey at the time of the study which did not display any abnormality.

The proband had 2 children with a non-related, healthy woman. She had no personal or familiar history of bone disorders and also underwent a skeletal survey that was normal.

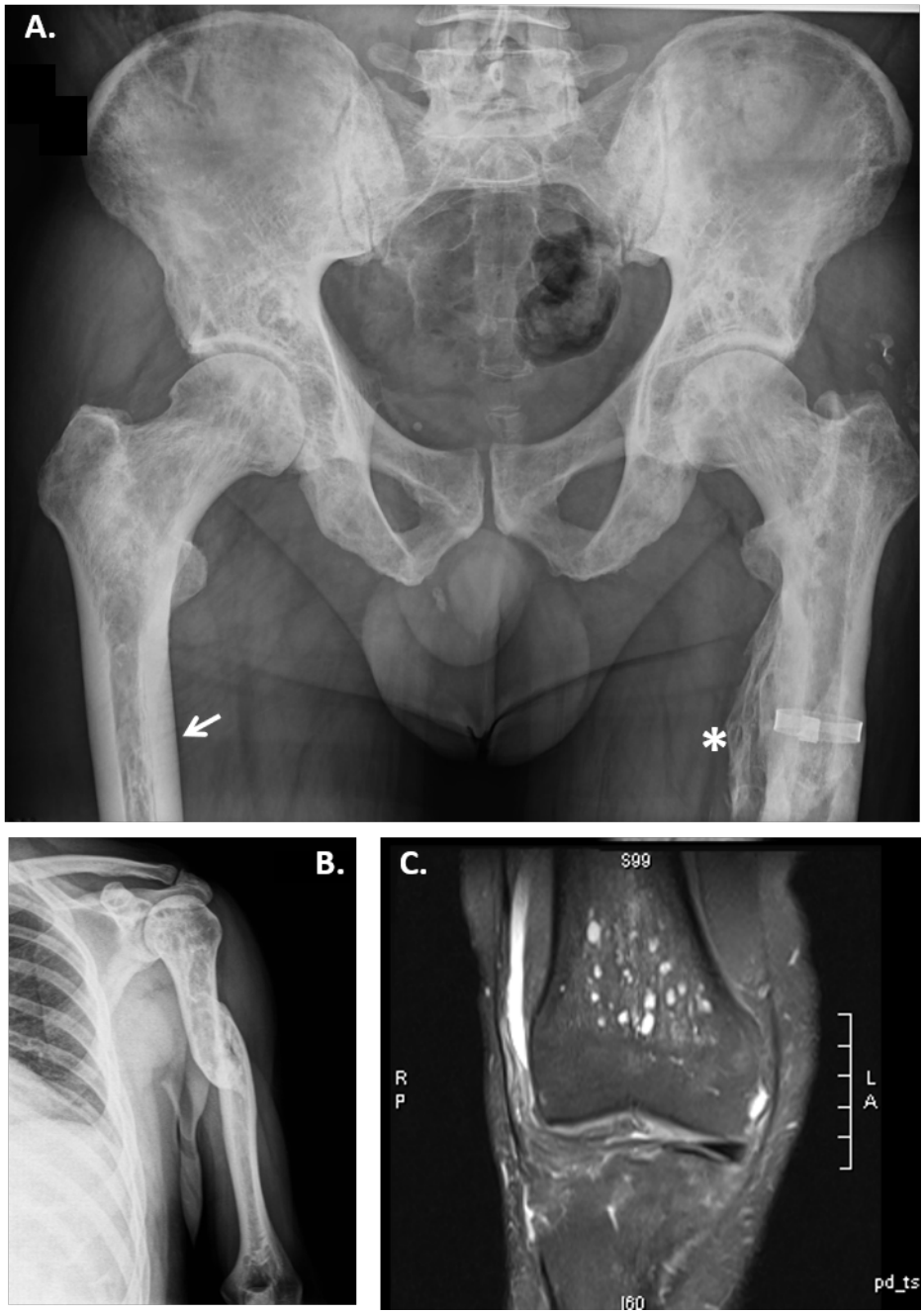

Figure 2. Proband's radiographic imaging. A. Pelvis and proximal femurs. Widespread bone rarefaction is noted at all displayed sites. An abnormal periostic reaction is observed around the fractured site at the left femoral diaphysis (asterisk). Femoral cortices are thickened (arrow). B. Left humeral fracture after a car accident. Bone rarefaction is observed throughout the humerus. C. Right knee MRI. Small lucent lesions are observed at the distal femoral metaphysis.

3.3 Son

The first child was a boy, 21 years of age at the time of the study. Skeletal abnormalities were first detected at age 14 after sustaining a small left olecranon fracture due to a fall from his own height. X-rays revealed lucent lesions at the distal left humeral diaphysis and metaphysis and proximal left ulnar and radial metaphysis (Figure 3A and 3C). Imaging of the right upper extremity showed similar lesions (Figure 3B). Pelvic and hip X-rays showed diffuse cortical thickening at both femurs in addition to lucent lesions at the femoral necks (Figure 3D). MRI imaging revealed altered signaling and similar lesional images at the clavicles, acromion, ribs and thoracic vertebrae. The initial suspicion was that of polyostotic fibrous dysplasia (PFD), but it was ruled out after a bone scan did not evidence any pathologic uptake, besides that of the fracture. The remaining study for McCune-Albright syndrome (MAS) screening was also negative, as no hormonal disturbances or café-au-lait spots were detected. Calcium, phosphorus, and PTH were within the normal range for his age, except for a mild alkaline phosphatase elevation. He reported transient episodes of bone pain during adolescence which were attributed to growth spurts.

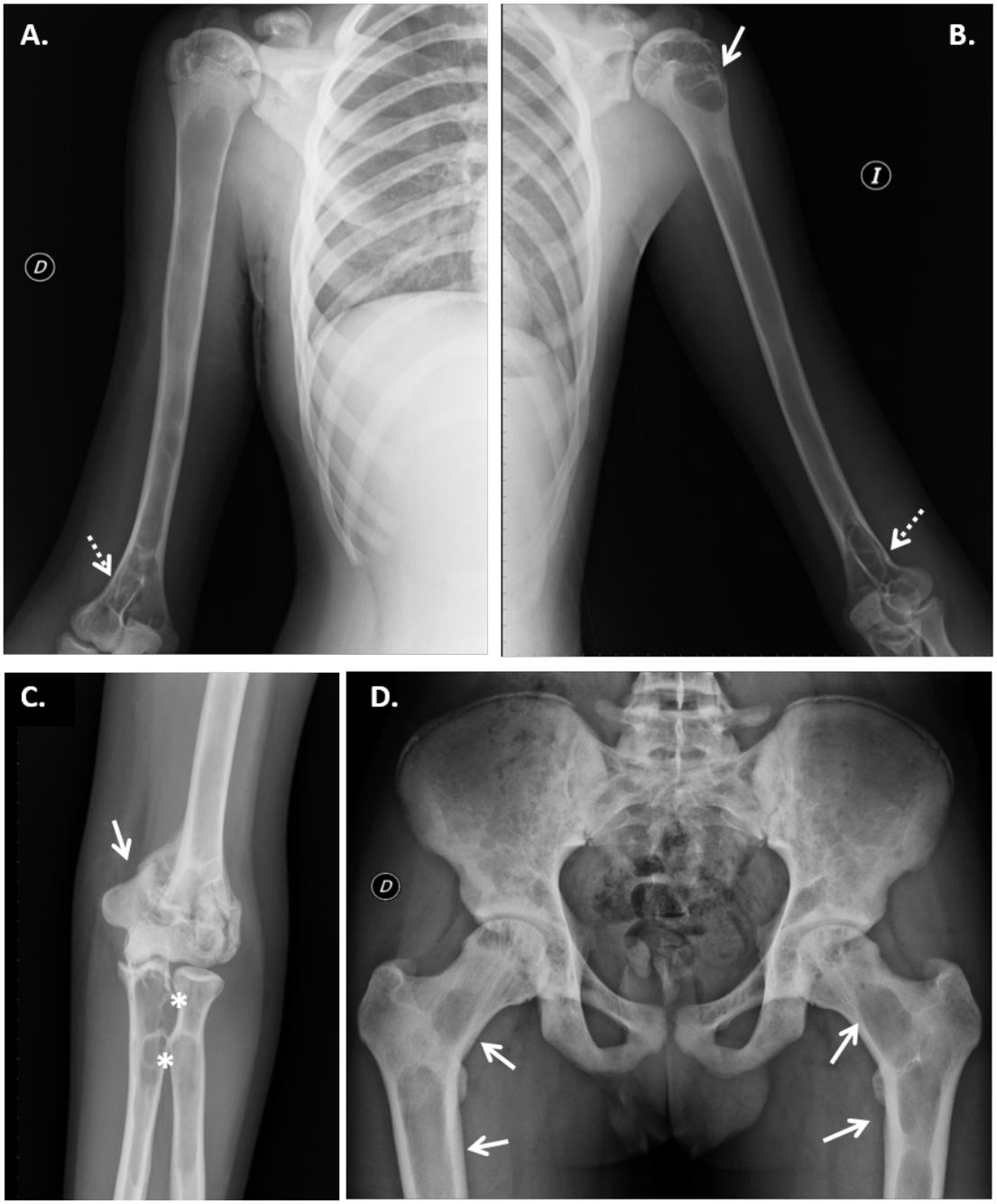

Figure 3. Proband's son radiographic imaging. A-B. Bilateral humeri showing extensive lucent lesions affecting entirely both diaphyses with secondary cortical thinning. Lucent lesions are also observed bilaterally at proximal and distal epiphyses, bilateral distal metaphyses, and proximal left metaphysis (arrow). Lesions appear particularly trabeculated at the distal humeri (dotted arrows). C. Right elbow. The site of an old olecranon fracture is observed (arrow) as well as trabeculated lucent lesions at the proximal ulnar and radial metaphyses (asterisks). D. Lucent lesions affecting both femoral necks and femoral diaphyses (arrows).

3.4 Daughter

The second child was a girl, 19 years of age at the time of the study. Dysplastic skeletal abnormalities were first detected at 15 years of age after she underwent X-ray imaging in the setting of idiopathic scoliosis (IS) evaluation. In addition to the scoliotic curve, X-rays revealed vertebrae of hyperostotic appearance (Figure 4A), which was further confirmed by a subsequent spinal MRI. Additional X-rays also identified distal metaphyseal and medullar lucent lesions that led to cortical diaphyseal thinning at the mid-distal humeri (Figure 4A, 4B, and 4C). Pelvic and hip X-rays showed marked cortical thickening of the femurs (Figure 4A). PFD and MAS were initially suspected. However, given that a bone scintigraphy did not reveal increased uptake at any site and that a complete endocrine panel did not show hormonal disturbances, that diagnosis was excluded. A thyroid US did display a mildly heterogenous gland due to the presence of colloidal cysts at both thyroid lobes. Thyroid function was normal and thyroid autoantibodies, including anti-thyroid peroxidase, anti-thyroglobulin, and TSH receptor antibodies, were negative. Blood tests showed moderate thrombocytopenia which was later found to be associated with hepatosplenomegaly. These manifestations were transient and she was finally diagnosed with idiopathic thrombocytopenic purpura (ITP) by the Hematology department at her local hospital. An innocent heart murmur was also detected. Cardiologists ruled out any structural heart disease after performing pertinent testing.

Figure 4. Proband's daughter radiographic imaging. A. Whole spinal and pelvic X-ray. Thoracolumbar scoliosis. Vertebrae display a sclerotic appearance. A large lucent lesion affecting the mid-distal right humeral diaphysis and distal metaphysis is observed. Trabeculation of the lesion is observed in the distal humeral metaphysis (arrow). Bilateral pelvic iliums show several microcystic lesions (asterisks). Bilateral femoral cortical thickening. Lucent lesions are absent at the femoral necks. B. Left humerus displaying a mid-diapaphyseal to distal metaphyseal/epiphyseal lucent lesion with secondary cortical thinning. C. Right elbow displaying trabeculated lesions similarly to those observed in her brother, while the ulnae and radius appear unaffected.

3.5 Physical Exam (PE)

PE was completely normal in the proband, children's mother, and son i.e., no dysmorphic facial features, abnormal intraoral features, body asymmetries or disproportions, or cutaneous lesions were identified. Mild hepatomegaly and thoracolumbar prominence corresponding to the scoliotic curvature were detected in the daughter. Proband's weight was 105 kg and height 181 cm. Children's mother height was 170 cm. Son's weight was 98 kg and height 192 cm. Daughter's weight was 69 kg and height 178 cm.

3.6 Impact Microindentation

BMSi values were elevated in the proband, and his son and daughter: BMSi (mean ± SD) was 83 ± 2.3, 82.3 ± 2.5, 87.7 ± 3.45, respectively, indicating above average bone mechanical properties.

3.7 DXA

DXA results are displayed in Table 1. Briefly, BMD values were very elevated in father and daughter. The son displayed BMD values on the high end of normality at the spine and normal at the hip, a site that also presented with extensive lucent lesions (Figure 3D). BMD was within the normal range at all sites in the proband's brother and in the wife's lumbar spine, while it displayed osteopenia in her hip and femoral neck.

Table 1. DXA outcomes in studied individuals

Subjects	Lumbar spine		Femoral Neck		Total Hip	
	BMD g/cm^2	T-/Z-score	BMD g/cm^2	T-/Z-score	BMD g/cm^2	T-/Z-score
Proband (II.3)	1.416	3/3.5	1.722	5.8/6.7	1.620	5.9/7.5
Daughter* (III.3)	1.636	4.7	1.495	5.5	1.614	5.5
Son* (III.2)	1.363	2.4	0.836	-0.7	1.054	0.1
Brother (II.1)	1.109	0.2/0.9	0.814	-0.9/0.2	0.995	-0.2/0.3
Wife (II.4)	0.977	-0.6/0.6	0.653	-1.8/-0.6	0.732	-1.7/-0.9

*Only Z-scores were calculated for these individuals as they were 19 and 21 at the time of the study.

Family members are designated in relationship to the proband.

3.8 Mineral panel

Mineral panel results are displayed in Table 2. Briefly, the proband's son displayed elevated bone resorption and formation markers, while the daughter, after being subject to vitamin D replacement due to vitamin D deficiency detected in a prior blood test (results not shown), showed elevated BAP and P1NP, indicating a high bone turnover/bone formation state, respectively. Conversely, the proband, displayed low BAP and OC levels, while P1NP and CTX were in low end of normality. The proband´s wife exhibited high bone formation markers in the setting of a probable primary hyperparathyroidism (her serum calcium was at the high end of normality) that is currently under study. Serum calcium and phosphate and kidney function were normal in all.

Table 2. Mineral panel in affected and unaffected individuals

	ALP (U/L)	BAP (µg/L)	PTH (pg/ml)	OC (ng/ml)	CTX (pg/ml)	P1NP (ng/ml)	Vit D (deficiency <10ng/ml; suboptimal 10-30 ng/ml))
Proband (II.3)	61 (40-150)	**7** (9-15)	93 (14-100)	**11,2** (14-46)	260 (90-840)	27 (23.3-94.4)	30
Daughter (III.3)	55 (50-175)	**13** (6-10)	43 (14-100)	35,1 (11-43)	**391** (40-540)	**119** (15-58.9)	**87**
Son (III.2)	135 (40-150)	**29** (9-15)	50 (14-100)	28,2 (24-70)	**725** (90-580)	**132** (23,3-94,4)	**24**
Brother (II.1)	54 (40-150)	10 (9-15)	76 (14-100)	15,7 (14-46)	300 (90-840)	38 (23,3-94,4)	**21**
Wife (II.4)	102 (35-120)	**22** (10-16)	**180** (14-100)	**49,1** (11-43)	774 (40-730)	**105** (15-58.6)	**22**

Normality ranges for each parameter are displayed adjusted for sex and age in parenthesis. Altered values are bolded and underlined. Family members are designated in relationship to the proband.

Abbreviations: ALP: tissue non-specific alkaline phosphatase, **BAP**: bone specific alkaline phosphatase, **PTH**: parathormone, **OC**: osteocalcin, **CTX**: C-terminal

telopeptide of type 1 collagen, **P1NP**: procollagen type 1 N propeptide, **Vit D**: vitamin D

3.9 WES results and *in silico* analysis

Variant filtering yielded a total of 26 rare variants shared by the affected individuals and absent in the unaffected family members (Table 3). Matchmaker Exchange did not retrieve any of the specific variants we submitted. In addition, uploaded clinical data from patients with different variants in our candidate genes did not reveal any kind of phenotypic correlation with our cases, with the exception of *ODF2*, which was identified in another patient with non-defined neurologic and skeletal involvement. However, current available data indicate that *ODF2*, which encodes a key component of sperm tail outer dense fibers and has been linked to male infertility [12], is not associated with bone biology. Potential implication of remaining variants in mineral metabolism and skeletal disorders was investigated in public sites including the Musculoskeletal Knowledge Portal, GeneCards, and PubMed. Five of the investigated variants were identified in genes with a potential role in bone biology: *SEMA4D, TBX18, PTCH1, PTK7* and *ADGRE5.* Of these, two variants, p.(V212M) in *SEMA4D* and p.(R349Q) in *TBX18,* stood out as the most likely candidates given their putative role in bone biology and development. In addition, both variants displayed the highest predicted pathogenicity, i.e. CADD score of 23.1 and 28 respectively, and were considered to be deleterious by SIFT and probably damaging by PolyPhen (Table 3). Nonetheless, the predicted pathogenicity for p.(D436N) in *PTCH1*, p.(T683M) in *PTK7*, and p.(E724G) in ADGRE5 was not negligible either with CADD scores >20, and thus were also considered as possible contributors to the observed phenotype (Table 3).

399 Table 3. Rare variants shared by affected individuals and absent in the two non-affected
400 family members

Gene	Protein	Variant[1]	Effect on the protein	dbSNP[2]	Conservation[3]	Sift[4]	Polyphen[5]	CADD[6]
AC127029.3	Uncha-racterized Protein	chr17: 63917846 C>T	p.(A217T) Missense	rs373958758	1	0.64	0	10,3
ADGRE5	Adhesion G Protein-Coupled Receptor E5	chr9: 14406924 A>G	p.(E724G) Missense	rs143056436	0,033	**0.02**	0.205	23,9
APBA2	Amyloid Beta Precursor Protein Binding Family A Member 2	chr15: 29054318 C>T	p.(A145V) Missense	rs765759759	0,654	0.29	0	10,5
ARL6	ADP Ribosylation Factor Like GTPase 6	chr3: 97788001 C>T	p.(R121C) Missense	rs202044896	0,998	**0**	**0.899**	34
ASXL3	ASXL Transcript-tional Regulator 3	chr18:33744091A>G	p.(M1415V) Missense	rs181303838	0,608	0.32	0	7,8
ATP6V1G2	ATPase H+ Transpor-ting V1 Subunit G2	chr6: 31546170 T>C	p.(Q41R) Missense	rs201901212	1	0.07	**0.862**	26,6
CACNA1A	Calcium Voltage-Gated Channel Subunit Alpha1 A	chr19: 13207562 CCCGCTG>C	p.Ser2429_Gly2430del In frame deletion	rs775428832				
DMAC2	Distal Membrane Arm Assembly Complex 2	chr19:. 41436446 T>C	p.(H87R)	rs566734225	0,017	**0**	0.131	15,8
DNAH11	Dynein Axonemal Heavy Chain 11	Chr7: 2174	p.(I2661T) Missense	rs372730542	1	**0**	0.187	23,9

		1994 T>C						
DNAH11	Dynein Axonemal Heavy Chain 11	chr7: 21711818 C>G	p.(A2314G) Missense	rs372541483	1	0.07	**0.999**	27
FAM171A1	Family With Sequence Similarity 171 Member A1	chr10: 15254801 G>T	p.(T166N) Missense	rs138799489	1	0.07	**0.955**	24,6
GNL1	G Protein Nucleolar 1	chr6: 30555078 C>T	p.(R118Q) Missense	rs762035615	0,002	0.57	0	3,3
GPR63	G protein coupled receptor 63	chr6: 96799296 G>A	p.(R146*) Nonsense					
KRI1	KRI1 Homolog	chr19: 10557617 C>T	p.(D524N) Missense	rs142840947	0,999	**0.02**	**0.988**	26,2
LRRC30	Leucine Rich Repeat Containing 30	chr18:723118 8G>A	p.(R17K) Missense	rs200142671	0,13	0.9	0	6
MDH1B	Malate Dehydrogenase 1B	chr2: 20675530 3G>A	p.(R206C) Missense	rs145046021	0,006	0.18	**0.676**	14
ODF2	Outer Dense Fiber Of Sperm Tails 2	chr9: 12850011 0G>A	p.(R782H) Missense	rs201020349	0,997	**0**	**0.988**	32
POLE	DNA Polymerase Epsilon, Catalytic Subunit	chr12: 132624738 8G>C	p.(L2274V) Missense	rs148788180	0,999	1	0	13,2
PTCH1	Patched 1	chr9: 95478096 C>T	p.(D436N) Missense	rs142274954	0.998	0.12	0.066	22.8
PTK7	Protein Tyrosine Kinase 7	chr6: 43142276 C>T	p.(T683M) Missense	rs796441111	0.755	0.15	**0.671**	23

RBSN	Rabenosyn, RAB Effector	chr3: 150960 21 C>G	p.(E34Q) Missense	rs141479781	1	0.07	**0.996**	24
SEMA4D	Semaphorin 4D	chr9: 893914 04 C>T	p.(V212M) Missense	rs377565599	0,998	**0**	**0.981**	22,9
SLC22A18	Solute Carrier Family 22 Member 18	chr11: 292245 1G>A	p.(V328I) Missense	rs148838489	0,046	0.17	0.024	11,6
TAPBP	TAP Binding Protein	chr6: 333038 29 C>G	p.(W487C) Missense	rs145837211	0,001	0.26	0.001	8,2
TBX18	T-Box Transcription Factor 18	chr6: 847385 50 C>T	p.(R349Q) Missense	rs187085991	1	**0.02**	**0.983**	29

Genes are listed in alphabetical order.
[1]Genomic position of the variant in the human reference genome GRCh38
[2]Reference SNP ID number (rs) and MAF (minor allele frequency) for the already described variants
[3]Conservation score in vertebrates from PhastCons (0,000 to 1), being 1 the most conserved locus.
[4]Sift: 0-0.05 damaging (in bold); 0.051-1 tolerable (non-damaging)
[5]PolyPhen: 0-0.4 benign; 0.41-0.89 possibly damaging; 0.9-1 pathogenic (in bold)
[6]CADD: the greater the score, the more damaging the variant is predicted to be

4. DISCUSSION

Here we present a familial case of a previously unreported skeletal dysplasia characterized by HBM and bone lesions, that underwent extensive clinical phenotyping and genetic analysis through WES. The affected family members included the proband and his two children, a boy and a girl, suggesting that the dysplasia followed an autosomal dominant inheritance pattern. WES was performed in the three affected members and in two unaffected relatives, the proband's brother and his non-consanguineous wife (and mother of the affected children), allowing us to filter for rare variants that were only present in the cases. Genetic variants were identified in genes that are known to play a role in bone metabolism, but that have not been previously linked to a metabolic bone

disorder including *TBX18, SEMA4D,* and *ADGRE5*. Rare variants in *PTCH1* and *PTK7*, which have been previously associated with other skeletal diseases, were also found.

Unlike other HBM disorders characterized by debilitating symptoms, the dysplasia in this family was paucisymptomatic. In the case of the proband, skeletal anomalies were incidentally identified during radiographic exams at age 36 after a high-impact traumatic event. In the daughter's case, the dysplasia was also fortuitously detected through X-rays during medical evaluation for idiopathic scoliosis. Perhaps the most symptomatic individual was the proband's son, who did report periods of intermittent bone pain during growth, as well as a low-impact fracture at the olecranon, a skeletal site that displayed several lucent lesions and secondary cortical thinning. He was also the affected member with the most extensive disease and the lowest BMD, particularly at the hip and femoral neck, but again, lucent lesions were also present at this site which, very probably, exerted a densitometric-lowering effect. In contrast to his children, the proband exhibited skeletal rarefaction at several sites which we suspect is an age-related process as similarly occurs in fibrous dysplasia [13].

An unresolved aspect is whether the elevated bone mass in these individuals is the consequence of increased bone formation or defective bone resorption. The absence of fragility fractures (except for the mild olecranon fracture in the son) and high BMSi values obtained with the microindentation technique (which indicate that the indented bone had good mechanical properties), suggest that the skeletal phenotype is probably the result of a supraphysiological bone-forming effect. Bone turnover markers were not too informative on this aspect as they were elevated in the proband's children while they were low or on the low-end of normality in the proband. Besides transient thrombocytopenia associated with hepatosplenomegaly, later classified as ITP, and mild structural thyroid abnormalities in the daughter, no extra-skeletal abnormalities were identified. This suggests that the implicated variants had a skeletal-specific effect. Of the identified rare variants, p.(V212M) in *SEM4AD* and p.(R349Q) in *TBX18* appeared as the most likely candidates due to their comparatively high pathogenicity scores and presumed role in skeletal biology.

SEMA4D encodes semaphorin 4D (SEMA4D), a member of the highly conserved semaphorin protein family [14]. SEMA4D has established roles in cancer biology (it

promotes neoplastic growth) and in immune system regulation, but recent evidence points to additional functions, including bone remodeling [14]. Both its membrane-bound and soluble forms bind to specific receptors, Plexin-B1 being its main receptor in non-immune cells. In bone, *in vitro* and animal studies have shown that Sema4d, which is produced and secreted by osteoclasts, binds to Plexin-B1, which is widely expressed by osteoblasts [14]. The Sema4d-Plexin-B1 complex results in altered osteoblastic differentiation and bone formation by suppressing insulin like growth factor (IGF1)-dependent signaling [15]. Negishi-Koga and collaborators generated a *Sema4d* KO mouse model which featured high bone mass, increased resistance to fracture in the three-point bending test, greater bone formation rate and normal osteoclastic activity, indicating that the osteosclerotic phenotype derived from enhanced osteoblastic bone formation [15]. Likewise, they generated a *Plexin-B1* KO that exhibited a similar bone phenotype. They also observed that in calvarial cells cultured in osteogenic conditions, Sema4d suppressed bone nodule formation and bone formation markers, including alkaline phosphatase, osteocalcin, and type I collagen. Furthermore, they evidenced that treatment with a blocking Sema4d antibody protected female ovariectomized mice from rapid bone loss. In agreement with Sema4d role in bone remodeling, a very recent study that conducted a genome wide meta-analysis in mesenchymal stem cells, evidenced significant upregulation of *ERBB2,* a downstream effector of SEMA4D/Plexin-B1 signaling, in cells derived from osteoporotic patients [16]. In a clinical setting, SEMA4D has been explored as a biomarker in osteoporosis, but existing evidence of its utility is conflicting [17, 18]. Segmental copy number loss of *SEMA4D* has also been identified in a substantial portion of patients with acetabular dysplasia, but functional analyses to explore potential causality have not been performed [19]. Collectively, data suggests that a defective copy of *SEMA4D*, whose quaternary structure is a homodimer, could lead to a dominant bone-forming effect.

TBX18 encodes T-Box Transcription Factor 18 (TBX18) which belongs to the T-box transcription factor family. It is known to play pivotal roles in organ formation during embryogenesis [21]. From a clinical standpoint, mutations in TBX18*,* which like SEMA4D is a homodimer, have been identified in dominant urinary tract malformations [22] and congenital heart defects [23]**.** In mouse models, both under- and overexpression of *TBX18* have resulted in severe skeletal ossification anomalies [24]**.** Subsequent animal studies have shown that through epigenetic mechanisms, *Tbx18* is

spatially and temporally expressed in cells of chondrocytic lineage involved pre- and postnatally in endochondral bone formation [25]. Given that lucent lesions observed in the affected individuals are close to the metaphyses and have appeared before growth plate fusion, it is plausible that altered TBX18 activity could have played a role in their development.

Another rare variant that could also contribute to the high bone mass phenotype is p.(E724G) in *ADGRE5.* The protein encoded by this gene is CD97, which belongs to the EGF-seven-span transmembrane (EGF-TM7) family of adhesion G protein coupled receptors (GPCRs) [26]. Most available data suggest that it plays a role in cell adhesion, leukocyte recruitment and migration as well as in immune responses given its high expression in inflammatory sites [26]**.** However, Won *et al*. also explored its potential role in bone biology by investigating a *CD97* KO mouse model, and found that CD97 played an important role in RANKL-mediated osteoclastogenesis [27]. In addition, they also observed an increase in bone mass in *CD97* KO mice as compared to WT which was secondary to decreased osteoclastic activity. Despite this potential implication in altered osteoclastic activity, it is unlikely that a single defective CD97 copy (CD97 forms a heterodimer) would be solely responsible for the elevated BMD values observed in this family. However, it may have contributed to it to a certain extent.

The two other remaining candidate variants were identified in genes *PTCH1* and *PTK7,* which are involved in the bone forming Wnt pathway. PATCHED1, the protein encoded by *PTCH1*, is a 12-pass transmembrane receptor that acts as hedgehog's (Hh) signaling main repressor [28]. The Hh signaling pathway, which also holds a key role in embryonic patterning, organ development, and cell proliferation, is a well-known positive regulator of Wnt-dependent bone formation [28]. Animal studies have shown that loss-of-function *Ptch1* mutations are associated with accelerated bone formation and increased bone mass [29]. Although perhaps PATCHED1is best known for its tumoral suppressor activity given its well-established role of Hh dysregulation in carcinogenesis. This is evident in patients with Gorlin syndrome, a rare condition characterized by the predisposition of neoplastic development at an early age, particularly basal cell carcinomas, odontogenic keratocysts of the jaws, and palmar pits among other abnormalities, that is caused by germline heterozygous loss-of-function *PTCH1* mutations [30]. None of these manifestations were encountered in our patients.

Also, while BMD has not been well-characterized in patients with Gorlin syndrome, a study indicated that it was above normal in the 2 subjects evaluated [29] but not close to the very high values seen in the family we studied. Furthermore, the identified p.(D436N) *PTCH1* variant has also been reported in 2 other studies, one associated with familial cases of Hirschsprung disease [31] and another with ocular developmental abnormalities [32] although causality of this variant with these disorders was not demonstrated. Skeletal findings were not reported in neither of these studies. In addition, both SIFT and Polyphen considered this variant probably benign, despite the CADD score of 23. While we cannot exclude a potential role for this variant in the cases, we do not consider it as the main candidate for the observed phenotype.

PTK7 encodes protein tyrosine kinase 7, a conserved transmembrane receptor [33]. It is unclear how PTK7 exactly signals, but there is broad evidence that it regulates Wnt signaling pathways [33]. PTK7 appears particularly relevant in the planar cell polarity (PCP) pathway, a non-canonical Wnt signaling pathway involved in cellular orientation and neural tube closure. Its involvement in canonical Wnt signaling is less clear although animal studies indicate that it attenuates β-catenin expression [34]. From a clinical standpoint, postnatal dysregulation of PTK7 activity has also been observed in cancer and metastatic development [35], although its mechanistic involvement remains unknown. Mutations in *PTK7* have also been involved in neural tube defects in humans [36] and interestingly, in idiopathic scoliosis (IS), which typically presents during adolescence and affects much more frequently girls than boys. Hayes and colleagues identified a rare *PTK7* heterozygous variant that was found to interfere with normal Wnt/PCP signaling in a boy with IS and no other evident abnormalities [37]. They also developed a zygotic mutant *Ptk7* zebrafish that displayed late onset spinal curvature without associated vertebral deformities, greatly resembling human IS. Importantly, vertebral mineral density was not found to be different between wild-type and mutant zebrafish. Going back to our case, data in the literature suggest that the *PTK7* mutation might have played a role in the development of IS in the daughter, while it appears less likely that it played a role on increased BMD.

Taking everything into consideration, we postulate that the encountered phenotype is the result of the effects of more than one variant. In relation to the high bone mass, it is plausible that it resulted from the additive effects of the *SEMA4D, PTCH1*, and *ADGRE5* variants, although we hypothesize that the *SEMA4D* variant, given its putative

role in bone formation, high predicted pathogenicity, and probable dominant effect, is the most highly contributing candidate. We also speculate that the *TBX18* variant is possibly responsible for the lucent bone lesions, while there is supporting data pointing to the role of the *PTK7* variant in the development of IS observed in the proband's daughter.

An important limitation from our study is the small number of affected individuals included in the study. This has led to a significant number of potential variants obtained from WES, making it difficult to ascribe the phenotype to a given mutation. In addition, we did not retrieve additional patients in public genomic databases with variants in the same genes and phenotypic correlation with our cases. Hence, functional tests to investigate the potential implication of each of the identified variants with the clinical manifestations must be performed. Furthermore, we have only explored coding regions in this family, thus, we cannot rule out that the observed phenotype is the result of (a) mutation(s) in intronic regions or due to epigenetic changes. We plan to to perform the pertinent genetic investigations to this end if we fail to obtain clear positive results from functional testing of our current candidate variants. Nonetheless, our study has important strengths, given that we present a novel familial skeletal dysplasia that has been extensively phenotyped and genetically investigated. In addition, the identification of putatively pathogenic variants in genes that have been previously associated with bone disorders in animal models such as *SEMA4D*, *ADGRE5* or *TBX18*, in the setting of a human skeletal dysplasia, might be great relevance to the field of bone metabolism. Future functional analysis of these variants will determine the importance of these genes in human skeletal physiology and perhaps discover new therapeutic targets for bone disorders.

5. ACKNOWLEDGEMENTS

This work was supported by the 2019 Translational Research Award from the Spanish Bone and Mineral Metabolism Research Foundation (FEIOMM2019) and by grant PID2019-107188RB-C21 from the Spanish Ministerio de Ciencia e Innovación. DO is a recipient of the Sara Borrell postdoctoral fellowship from the Instituto de Salud Carlos

III (Spanish Ministry of Health). The research was also supported by Centro de Investigación Biomédica en Red de Fragilidad y Envejecimiento Saludable (grant number CB16/10/00245), and European Regional Development Fund.

CRediT author statement

DO: conceptualization, methodology, investigation, resources, writing-original draft preparation, writing-reviewing and editing, supervision, visualization, funding acquisition, **NGG:** conceptualization, methodology, formal analysis, investigation, resources, data curation, writing-original draft preparation, **NMG, RR, SB, DG:** conceptualization, methodology, writing-original draft preparation, writing-reviewing and editing**, LPJ:** resources, investigation, writing-original draft, **XN:** resources, investigation, writing-original draft, **IEF:** resources, investigation, supervision, writing-original draft, writing-reviewing and editing, funding acquisition.

Funding: This work was supported by the 2019 Translational Research Award from the Spanish Bone and Mineral Metabolism Research Foundation (FEIOMM2019) and by grant PID2019-107188RB-C21 from the Spanish Ministerio de Ciencia e Innovación. DO is a recipient of the Sara Borrell postdoctoral fellowship from the Instituto de Salud Carlos III (Spanish Ministry of Health). The research was also supported by Centro de Investigación Biomédica en Red de Fragilidad y Envejecimiento Saludable (grant number CB16/10/00245), and European Regional Development Fund.

6. References

1. Boudin, E. and W. Van Hul, *Sclerosing bone dysplasias.* Best Pract Res Clin Endocrinol Metab, 2018. **32**(5): p. 707-723.
2. Bonafe, L., et al., *Nosology and classification of genetic skeletal disorders: 2015 revision.* Am J Med Genet A, 2015. **167A**(12): p. 2869-92.
3. Polyzos, S.A., T. Cundy, and C.S. Mantzoros, *Juvenile Paget disease.* Metabolism, 2018. **80**: p. 15-26.
4. Diez-Perez, A., et al., *Microindentation for in vivo measurement of bone tissue mechanical properties in humans.* J Bone Miner Res, 2010. **25**(8): p. 1877-85.

5. Diez-Perez, A., et al., *Technical note: Recommendations for a standard procedure to assess cortical bone at the tissue-level in vivo using impact microindentation.* Bone Rep, 2016. **5**: p. 181-185.
6. McLaren, W., et al., *The Ensembl Variant Effect Predictor.* Genome Biol, 2016. **17**(1): p. 122.
7. Sobreira, N.L.M., et al., *Matchmaker Exchange.* Curr Protoc Hum Genet, 2017. **95**: p. 9 31 1-9 31 15.
8. Kumar, P., S. Henikoff, and P.C. Ng, *Predicting the effects of coding non-synonymous variants on protein function using the SIFT algorithm.* Nat Protoc, 2009. **4**(7): p. 1073-81.
9. Adzhubei, I., D.M. Jordan, and S.R. Sunyaev, *Predicting functional effect of human missense mutations using PolyPhen-2.* Curr Protoc Hum Genet, 2013. **Chapter 7**: p. Unit7 20.
10. Rentzsch, P., et al., *CADD: predicting the deleteriousness of variants throughout the human genome.* Nucleic Acids Res, 2019. **47**(D1): p. D886-D894.
11. Siepel, A., et al., *Evolutionarily conserved elements in vertebrate, insect, worm, and yeast genomes.* Genome Res, 2005. **15**(8): p. 1034-50.
12. Ito, C., et al., *Odf2 haploinsufficiency causes a new type of decapitated and decaudated spermatozoa, Odf2-DDS, in mice.* Sci Rep, 2019. **9**(1): p. 14249.
13. Kushchayeva, Y.S., et al., *Fibrous dysplasia for radiologists: beyond ground glass bone matrix.* Insights Imaging, 2018. **9**(6): p. 1035-1056.
14. Lontos, K., et al., *The Role of Semaphorin 4D in Bone Remodeling and Cancer Metastasis.* Front Endocrinol (Lausanne), 2018. **9**: p. 322.
15. Negishi-Koga, T., et al., *Suppression of bone formation by osteoclastic expression of semaphorin 4D.* Nat Med, 2011. **17**(11): p. 1473-80.
16. Hasan, L.K., et al., *Metaanalysis Reveals Genetic Correlates of Osteoporosis Pathogenesis.* J Rheumatol, 2020.
17. Anastasilakis, A.D., et al., *Circulating semaphorin-4D and plexin-B1 levels in postmenopausal women with low bone mass: the 3-month effect of zoledronic acid, denosumab or teriparatide treatment.* Expert Opin Ther Targets, 2015. **19**(3): p. 299-306.
18. Zhang, Y., et al., *Serum Sema4D levels are associated with lumbar spine bone mineral density and bone turnover markers in patients with postmenopausal osteoporosis.* Int J Clin Exp Med, 2015. **8**(9): p. 16352-7.
19. Sekimoto, T., et al., *Segmental copy number loss in the region of Semaphorin 4D gene in patients with acetabular dysplasia.* J Orthop Res, 2013. **31**(6): p. 957-61.
20. Zhu, L., et al., *Regulated surface expression and shedding support a dual role for semaphorin 4D in platelet responses to vascular injury.* Proc Natl Acad Sci U S A, 2007. **104**(5): p. 1621-6.
21. Farin, H.F., et al., *T-box protein Tbx18 interacts with the paired box protein Pax3 in the development of the paraxial mesoderm.* J Biol Chem, 2008. **283**(37): p. 25372-25380.
22. Vivante, A., et al., *Mutations in TBX18 Cause Dominant Urinary Tract Malformations via Transcriptional Dysregulation of Ureter Development.* Am J Hum Genet, 2015. **97**(2): p. 291-301.
23. Dias, R.R., et al., *Holt-Oram syndrome presenting as agenesis of the left pericardium.* Int J Cardiol, 2007. **114**(1): p. 98-100.
24. Bussen, M., et al., *The T-box transcription factor Tbx18 maintains the separation of anterior and posterior somite compartments.* Genes Dev, 2004. **18**(10): p. 1209-21.
25. Haraguchi, R., R. Kitazawa, and S. Kitazawa, *Epigenetic regulation of Tbx18 gene expression during endochondral bone formation.* Cell Tissue Res, 2015. **359**(2): p. 503-512.

26. Gray, J.X., et al., *CD97 is a processed, seven-transmembrane, heterodimeric receptor associated with inflammation.* J Immunol, 1996. **157**(12): p. 5438-47.
27. Yeon Won, H., et al., *Contradictory Role of CD97 in Basal and Tumor Necrosis Factor-Induced Osteoclastogenesis In Vivo.* Arthritis Rheumatol, 2016. **68**(5): p. 1301-13.
28. Ingham, P.W. and A.P. McMahon, *Hedgehog signaling in animal development: paradigms and principles.* Genes Dev, 2001. **15**(23): p. 3059-87.
29. Ohba, S., et al., *Patched1 haploinsufficiency increases adult bone mass and modulates Gli3 repressor activity.* Dev Cell, 2008. **14**(5): p. 689-99.
30. Gorlin, R.J., *Nevoid basal-cell carcinoma syndrome.* Medicine (Baltimore), 1987. **66**(2): p. 98-113.
31. Luzon-Toro, B., et al., *Exome sequencing reveals a high genetic heterogeneity on familial Hirschsprung disease.* Sci Rep, 2015. **5**: p. 16473.
32. Chassaing, N., et al., *Targeted resequencing identifies PTCH1 as a major contributor to ocular developmental anomalies and extends the SOX2 regulatory network.* Genome Res, 2016. **26**(4): p. 474-85.
33. Berger, H., A. Wodarz, and A. Borchers, *PTK7 Faces the Wnt in Development and Disease.* Front Cell Dev Biol, 2017. **5**: p. 31.
34. Hayes, M., et al., *Ptk7 promotes non-canonical Wnt/PCP-mediated morphogenesis and inhibits Wnt/beta-catenin-dependent cell fate decisions during vertebrate development.* Development, 2013. **140**(8): p. 1807-18.
35. Tammela, T., et al., *[Urethral carcinoma in men--a difficult diagnostic problem].* Duodecim, 1989. **105**(9): p. 851-5.
36. Wang, M., et al., *Role of the planar cell polarity gene Protein tyrosine kinase 7 in neural tube defects in humans.* Birth Defects Res A Clin Mol Teratol, 2015. **103**(12): p. 1021-7.
37. Hayes, M., et al., *ptk7 mutant zebrafish models of congenital and idiopathic scoliosis implicate dysregulated Wnt signalling in disease.* Nat Commun, 2014. **5**: p. 4777.